CFD Modelling of Cavitation Phenomenon in Piston Ring/Cylinder Liner Conjunction

Hamed Shahmohamadi*, Ramin Rahmani, Homer Rahnejat and Colin P. Garner

Wolfson School of Mechanical and Manufacturing Engineering, Loughborough University, Loughborough, Leicestershire LE11 3TU, UK
*Corresponding author: h.shahmohamadi@lboro.ac.uk

1. Introduction

The basic function of the compression piston ring is to seal the combustion chamber. This prevents the escape of high-pressure gases and conversely lubricant leakage into the chamber. The piston ring assembly accounts for approximately 30-45% of engine frictional losses [1]. However, effective sealing function of the compressions ring can result in increased friction and thus parasitic losses, because of reduced ring-liner clearance. Therefore, in order to improve engine performance, it is important for tribologists to have a deep understanding of lubrication phenomena at the piston ring –cylinder liner interface.

The convergent-divergent conjunction between the piston ring profile and cylinder liner suggests that the oil film may experience cavitation. There are two possible cavitation patterns for a piston ring, i.e., enclosed cavitation and open cavitation [2, 3].

Enclosed cavitation assumes that the fluid film ruptures somewhere in the diverging outlet wedge of the conjunction and reforms before the trailing edge of the ring. Here, the lubricant flow reaches the exit pressure boundary condition. On the other hand, open cavitation assumes that the fluid film does not reform, but separates into striated flow in the diverging wedge. For a fully flooded piston ring, enclosed cavitation is very likely to occur. The investigations presented in this paper are focused on a fully flooded piston ring with the enclosed cavitation pattern.

In recent years, several researchers [4-6] used the JFO boundary conditions, coupled with the Elrod algorithm to obtain numerical solutions for hydrodynamically lubricated piston rings. However, the authors are not aware of any published work, which has employed JFO boundary conditions directly to obtain an analytical solution of the problem. This paper presents a novel CFD of piston ring lubrication problem with enclosed cavitation pattern under assumed isothermal condition. In addition to the obvious advantages of the CFD approach, it provides a better insight into the physics of problem.

2. Problem description and Governing Equations

A general schematic of the enclosed cavitation phenomenon in piston ring and cylinder liner conjunction is shown in Figure 1. The parabolic ring profile $h_s(x)$ is defined as:

$$h_s(x) = \frac{cx^2}{(b/2)^2} \quad (1)$$

where c and b are crown height and ring contacting face-width respectively. This simplifies the problem to a one dimensional contact, which is valid for ring-bore contact of bore diameter-to-ring face-width ratio: $2\pi r_0/b \geq 30$ as shown by Haddad and Tian [7], which is applicable to the engine studied here. The engine is a high performance V12 4-stroke naturally aspirated gasoline engine with specifications provided in Table 1.

During most of the engine cycle there is no localised contact deflection and the ring–liner conjunction operates under hydrodynamic or mixed regimes of lubrication [8].

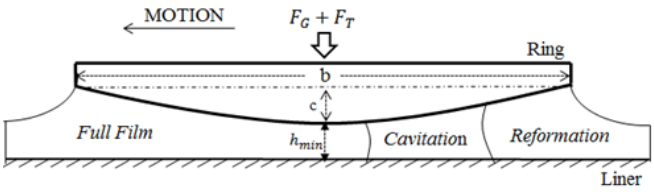

Figure1: 2D Diagram of piston ring–liner conjunction

Table1: Engine data [1]

Parameters	Values	Units
Crank-pin radius, r	40	mm
Connecting rod length, l	141.9	mm
Bore nominal radius, r_0	44.45	mm
Ring crown height, c	14.9	µm
Ring axial face-width, b	1.475	mm
Ring radial width, d	3.5	mm
Ring free end gap, g	10.5	mm
Engine speed, N	2000	rpm

The contact is divided into three distinct regions: (i) full film, (ii) film rupture and cavitation and (iii)

lubricant film reformation. To describe the physics of fluid flow in the cavitated region, in which two state phases of lubricant co-exist at the same time, a suitable two-phase flow model needs to be employed alongside the Navier-Stokes equations.

The fluid flow is governed by the 2D compressible Navier–Stokes equations. The continuity of flow is given as:

$$\frac{D\rho}{Dt} = -\rho\left(\frac{\partial u}{\partial x} + \frac{\partial w}{\partial z}\right) \tag{2}$$

and the conservation of momentum provides:

$$\frac{Du}{Dt} = \frac{1}{\rho}\left[\eta\left(\frac{\partial^2 u}{\partial x^2} + \frac{\partial^2 u}{\partial z^2} + \frac{1}{3}\left(\frac{\partial^2 u}{\partial x^2} + \frac{\partial^2 w}{\partial x \partial z}\right)\right) - \frac{\partial p}{\partial x}\right] \tag{3}$$

$$\frac{Dw}{Dt} = \frac{1}{\rho}\left[\eta\left(\frac{\partial^2 w}{\partial x^2} + \frac{\partial^2 w}{\partial z^2} + \frac{1}{3}\left(\frac{\partial^2 u}{\partial x \partial z} + \frac{\partial^2 w}{\partial z^2}\right)\right) - \frac{\partial p}{\partial z}\right] \tag{4}$$

where $\frac{D}{Dt}$ is the total derivative with respect to time t, ρ is the lubricant density, η is the effective lubricant dynamic viscosity, p is pressure, u the x-component of velocity (direction of lubricant entraining motion) and v the y-component of velocity. One possibility in a CFD model is to evaluate fluid viscosity as a function of pressure and temperature along the liner and into the depth of the lubricant film. The following boundary conditions are used along the axial x-direction of the contact (i.e. along the ring face-width)

$$\begin{aligned} p(-b/2) &= p_L \\ p(+b/2) &= p_U \\ p(x_c) &= p_c \end{aligned} \tag{5}$$

Table2. Lubricant properties [9]

Parameters	Values	Units
Lubricant viscosity, η	0.0069	kg/m-s
Lubricant density, ρ	0.87	kg/m^3

3. The cavitation Model: Vapour Mass Fraction

The lubricant is assumed to be a mixture of liquid and vapour. A vapour transport equation governs the vapour mass fraction, f, given as:

$$\frac{\partial}{\partial t}(\rho_m f) + \nabla(\rho_m \vec{v}_\upsilon f) = \nabla(\chi \nabla f) + R_e - R_c \tag{6}$$

where ρ_m is the mixture density, $\vec{v}_\upsilon$ is the velocity vector of the vapour phase, χ is the effective exchange coefficient, and R_e and R_c are the vapour generation and condensation rates (or phase change rates). The rate expressions are derived from the Rayleigh-Plesset equations and limiting bubble size considerations (interface surface area per unit volume of vapour) [10]. These rates are functions of the instantaneous local static pressure and are given as:

When: $p < p_{sat}$

$$R_e = C_e \frac{V_{ch}}{\gamma} \rho_l \rho_\upsilon \sqrt{\frac{2(p_{sat} - p)}{3\rho_l}}(1 - f) \tag{7}$$

When: $p > p_{sat}$

$$R_c = C_c \frac{V_{ch}}{\gamma} \rho_l \rho_\upsilon \sqrt{\frac{2(p - p_{sat})}{3\rho_l}}\, f \tag{8}$$

where the suffices l and υ denote the liquid and vapour phases, V_{ch} is a characteristic velocity, γ is the surface tension of the liquid, p_{sat} is the liquid saturation vaporisation pressure at the given temperature, and C_e and C_c are empirical constants, in this case with the values 50 and 0.01 respectively [11].

4. SIMULATION METHOD

CFD package FLUENT 14.0 is used to develop a 2D simulation model. The pre-processor Ansys Design Modeller and Meshing is applied for the grid generation. Owing to the very thin lubricant film, particularly relative to the ring diameter and length, only hexahedral elements are used. Forty divisions are used across the film thickness and 1500 divisions along the ring contacting face-width. This provides a total number of cells of 60,000. Reynolds' number is set to laminar flow conditions. The vaporisation pressure is assumed to be the atmospheric pressure.

Pressure inlet and outlet boundary conditions are used for the leading and trailing edges of the ring/liner contact. Therefore, when the piston undergoes upstroke motion, the inlet pressure is that of the combustion chamber, whilst at the exit the crank-case pressure is assumed to be at atmospheric. In addition, for the down-stroke sense of the piston, the inlet pressure is set to that of the crank-case (atmospheric) pressure, whilst the outlet pressure is that of the combustion chamber.

The pressure-based mixture model is chosen for the present CFD analysis. The velocity–pressure coupling is treated using the SIMPLE algorithm and the second-order upwind scheme is used for momentum. For greater accuracy, a value of 10^{-6} is used for all residual terms.

In its radial plane, the ring is subjected to two outward forces: ring tension or elastic force F_T and the gas force F_G. These forces strive to conform the ring to the bore surface. Thus, the total outward force on the ring is $F = F_T + F_G$. The ring tension force is obtained as $F_T = p_e b r_0$, where the elastic pressure p_e is [12]

$$p_e = \frac{gEI}{3\pi b r_0^4} \tag{9}$$

where g is the ring end-gap in its free state. The gas force acting behind the ring's inner peripheral face is given by equation (22). The combustion pressure varies with engine speed and throttle demand.

$$F_G(\theta) = p_{gb}(\theta) b r_0 \tag{10}$$

where θ denotes polar angles at which the

measurements have taken place. These outward forces are opposed by the contact force generated as the result of combined actions of conjunctional hydrodynamic pressures and the load share carried by direct contact of surface asperities.

Two compiled user-defined functions (UDF) in the C programing language are used. The first UDF is used to compute the equilibrium position of the ring when a known external force is applied to it. The UDF integrates all pressure forces at the contact interface, taking into account the boundary conditions. The integrated pressure distribution is:

$$W(\varphi) = \int pdA \qquad (11)$$

The aforementioned quasi-static balance of applied forces on the ring is sought through:

$$Err_{load} = \frac{|F(\varphi) - W(\varphi)|}{F(\varphi)} \leq 10^{-3} \qquad (12)$$

The smoothing mesh method is used with a convergence tolerance of 10^{-5}. The dynamic mesh zones defined are: (a) the liner as "stationary", (b) interior face as "deforming" with "spring smoothing" method, and (c) the ring as "rigid body". The second UDF is applied to the fluid properties as functions of pressure.

5. Results

Figs. 2 and 3 show the lubricant film pressure distribution and oil-film thickness in the vicinity of the power stroke TDC (-5° and +10° of crank angle), predicted by three different algorithms. The minimum film thickness is smaller in the Elrod model. Therefore, the predicted maximum pressure is greater compared withthe other two models. The estimated pressure distribution in the current analysis is in accordance with Reynolds' approach to a greater extent in the high pressure zone. However, the Reynolds' model fails to predict the pressure variation in the cavitation zone.

Fig. 4 illustrates the volume fraction of vapour and fractional film content at the crank angle of -5°. As it can be seen in the fractional film content graph, the current analysis predicts that the mixed fluid contains more oil in the proximity of ring, while there is more vapour adjacent to the liner surface. Consequently, cavitation is anticipated to commence on the surface of liner. Unlike the CFD approach, the Elrod model estimates 100% vapour in the cavitation zone.

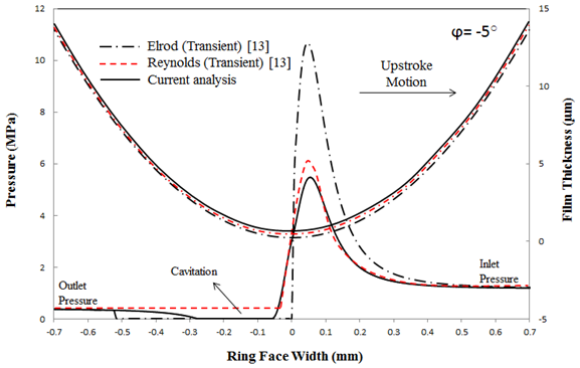

Figure2: Pressure distribution along the contact at crank angle of φ= -5°

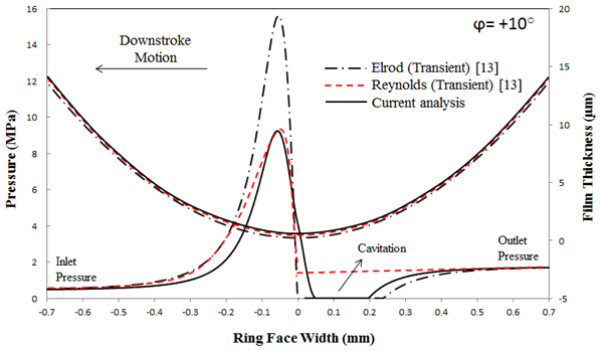

Figure3: Pressure distribution along the contact at crank angle of φ= 10°

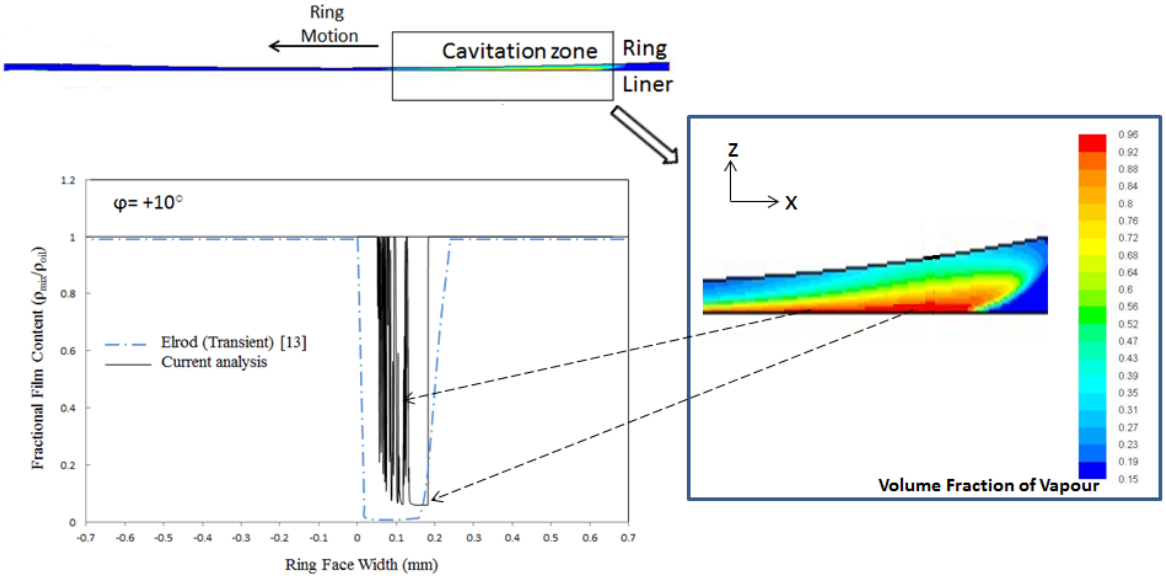

Figure4: Fractional film content and volume fraction of vapour at crank angle of φ= 10°

Acknowledgements

The authors would like to express their gratitude to the Lloyds Registry Educational Foundation (LREF) for the financial support extended to this research. Thanks are also due to the Engineering and Physical Sciences Research Council for the Encyclopaedic Program Grant, from which some of the research are used in this paper.

References

[1] Jeng, Y., "Theoretical Analysis of Piston Ring Lubrication-Part I: Fully Flooded Lubrication," *Trib. Trans.*, 35.4, 1992, 696-706.

[2] Ma, M. T., Smith, E. H., and Sherrington, I., "A Three-dimensional Analysis of Piston Ring Lubrication, Part I: Modelling," in *Proc. IMechE., Part J: J. Engng. Trib.*, 209, pp 1-14, (1995).

[3] Ma, M. T., Sherrington, I. and Smith, E. H., "Implementation of an Algorithm to Model the Starved Lubrication of a Piston Ring a Distorted Bores: Prediction of Oil Row and Onset of Gas Blow-by," in *Proc. IMechE, Part J: J. Engng. Trib*. 210, pp 29-44, (1996).

[4] Rahmani R., Theodossiades S., Rahnejat, H. and Fitzsimons B., "Transient elastohydrodynamic lubrication of rough new or worn piston compression ring conjunction with an out-of-round cylinder bore", *Proc. IMechE, Part J: J. Engng. trib., 226(4), 2012, pp. 284-305*

[5] Morris N., Rahmani R., Rahnejat H., King P.D. and Fitzsimons, B., "The influence of piston ring geometry and topography on friction", *Proc. IMechE, Part J: J. Engng. trib., 2012, DOI: 10.1177/1350650112463534*

[6] Mishra P.C., Rahnejat H. and King P.D., "Tribology of the ring—bore conjunction subject to a mixed regime of lubrication", *Proc. IMechE, Part C: J. Mech. Engng. Sci., 223(4), 2009, pp. 987-998*

[7] Haddad S. D. and Tian K.-T. "An analytical study of offset piston and crankshaft designs and the effect of oil film on piston slap excitation in a diesel engine", *Mechanism and Machine Theory, 30 (2), 1995, pp. 271–284*

[8] Mishra P.C., Balakrishnan S. and Rahnejat H., "Tribology of compression ring-to-cylinder contact at reversal", *Proc. IMechE, Part J: J. Engng. Trib, 222(7), 2008, pp. 815-826*

[9] Yang Q, Keith TG. An elastohydrodynamic cavitation algorithm for piston ring lubrication, *Tribology Transactions, 38(1), 1995, 97–107*

[10] Singhal A.K., Li H.Y., Athavale M.M., and Jiang Y., "Mathematical Basis and Validation of the Full Cavitation Model", *ASME FEDSM'01, New Orleans, Louisiana, 2001*

[11] Kubota A, Kato H, Yamaguchi H., "A new modelling of cavitating flows: a numerical study of unsteady cavitation on a hydrofoil section", *J. Fluid Mech., 240, 1992, pp. 59–96*

[12] Bin Chik, A., and Fessler H., "Radial pressure exerted by piston rings", *J. Strain Anal Eng. Des. I, 2, 1966, pp. 165–171*

[13] Chong W.W.F., Teodorescu M. and Vaughan N.D., "Cavitation induced starvation for piston-ring/liner tribological conjunction", *Trib. Int., 44(4), 2011, pp. 483-497*

Nomenclature

A	contact area
b	ring axial face-width
C_e , C_c	empirical constants
d	ring thickness
F_G	gas force
F_T	ring elastic force
g	ring end gap
h_m	minimum film thickness
l	connecting rod length
L	ring peripheral length
p_{atm}	atmospheric pressure
p_c	cavitation/lubricant vaporisation pressure
p_e	elastic pressure
p	hydrodynamic pressure
r	crank-pin radius
r_0	nominal bore radius
R_e	vapour generation rate
R_c	vapour condensation rate
Re	Reynolds number
t	time
U	ring sliding velocity
$\vec{V}$	velocity vector
V_{ch}	characteristic velocity
x_c	oil film rupture point

Greek Symbols

φ	crank angle
η	lubricant dynamic viscosity
γ	surface tension
ρ	lubricant density
χ	effective exchange coefficient